MJF

14. Grant, S. *Am. J. Sci.* **290,** 261-294 (1990).
15. Conway Morris, S., Mattes, B. W. & Chen, M. *Am. J. Sci.* **290A,** 245-260 (1990).
16. Sokolov, B. S. & Iwanowski, A. B. (eds) *The Vendian System: Vol. 1 Paleontology* English edn (Springer, Berlin, 1990).
17. Hofmann, H., Narbonne, G. M. & Aitken, J. D. *Geology* **18,** 1199-1202 (1990).
18. Hambrey, M. B. & Harland, W. B. (eds) *Earth's Pre-Pleistocene Glacial Record* (Cambridge Univ. Press, Cambridge, 1981).
19. Harland, W. B. *Geol. Rundschau* **54,** 45-61 (1964).
20. Walter, M. R. (ed.) *Stromatolites* (Elsevier, Amsterdam, 1976).
21. Bertrand-Sarfati, J. & Walter, M. R. *Precambrian Res.* **15,** 353-371 (1981).
22. Walter, M. R. & Heys, G. R. *Precambrian Res.* **29,** 149-175 (1985).
23. Hofmann, H. J. *Geosci. Canada* **14,** 135-154 (1987).
24. Khomentovsky, A. A. in *The Vendian System Vol. 2 Regional Geology* English edn (eds Sokolov, B. S. & Fedonkin, M. A.) 102-183 (Springer, Berlin, 1990).
25. Gnilovskaya, M. B. (ed.) *Vendotaenids of the East European Platform* (Nauka, Leningrad, 1988).
26. Yin, L. *Palaeontologia Cathayana* **2,** 229-249 (1985).
27. Zang, W. & Walter, M. R. *Nature* **337,** 632-645 (1989).
28. Knoll, A. H. & Butterfield, N. J. *Nature* **337,** 602-603 (1989).
29. Vidal, G. *Palaeontology* **33,** 287-298 (1990).
30. Knoll, A. H. *Palaeontology* (in the press).
31. Moczydlowska, M. *Fossils Strata* **29,** 1-127 (1991).
32. Holser, W. T. in *Patterns of Change in Earth Evolution* (eds Holland, H. D. & Trendall, A. F.) 123-143 (Springer, Berlin, 1984).
33. Knoll, A. H., Hayes, J. M., Kaufman, A. J., Swett, K. & Lambert, I. B. *Nature* **321,** 832-838 (1986).
34. Fairchild, I. R. & Spiro, B. *Sedimentology* **34,** 973-988 (1987).
35. Kaufman, A. J., Hayes, J. M., Knoll, A. H. & Germs, G. J. B. *Precambrian Res.* **49,** 301-327 (1991).
36. Lambert, I. B., Walter, M. R., Zang, W., Lu, S. & Ma, G. *Nature* **325,** 140-142 (1987).
37. Fairchild, I. R., Marhall, J. D. & Bertrand-Sarfati, J. *Am. J. Sci.* **290A,** 46-79 (1990).
38. Aharon, P., Schidlowski, M. & Singh, I. B. *Nature* **327,** 699-702 (1987).
39. Derry, L. A., Keto, L. S., Jacobsen, S. B., Knoll, A. H. & Swett, K. *Geochim. cosmochim. Acta* **53,** 2331-2339 (1989).
40. Asmerom, Y., Jacobsen, S. B., Knoll, A. H., Butterfield, N. J. & Swett, K. *Geochim. cosmochim. Acta* **55,** 2883-2894 (1991).
41. Derry, L. A., Kaufman, A. J. & Jacobsen, S. B. *Geochim. cosmochim. Acta* (in the press).
42. Kirschvink, J. L., Magaritz, M., Ripperdam, R. L., Zhuravlev, A. Y. & Rozanov, A. Y. *GSA Today* **1,** 69-91 (1991).
43. Beanus, M. A. & Knauth, L. P. *Geol. Soc. Am. Bull.* **96,** 737-745 (1985).
44. Veizer, J., Compston, W., Clauer, N. & Schidlowski, M. *Geochim. cosmochim. Acta* **47,** 295-302 (1983).
45. Donnelly, T. H., Shergold, J. H., Southgate, P. N. & Barnes, C. N. in *Phosphorite Research and Development* (ed. Notholt, A. J. G. & Jarvis, I.) *Geol. Soc. Spec. Publ.* **52,** 273-287 (1990).
46. Kaufman, A. J., Jacobsen, S. B. & Knoll, A. H. *Earth planet. Sci. Lett.* (in the press).
47. Claypool, G. E., Holser, W. T., Kaplan, I. R., Sakai, H. & Zak, I. *Chem. Geol.* **28,** 199-260 (1980).
48. Ross, G. M., Bloch, J. D. & Krouse, H. R. *Abstr. Geol. Assoc. Canada/Miner. Assoc. Canada Ann. Mtg* **16,** 108 (1991).
49. Christie-Blick, N. *Mar. Geol.* **97,** 35-56 (1991).
50. Lindsay, J. F. *Am. Assoc. Petrol. Geol. Bull.* **71,** 1387-1403 (1987).
51. Lindsay, J. F. & Korsch, R. J. *Basin Res.* **2,** 3-25 (1989).
52. von der Borch, C. C., Christie-Blick, N. & Grady, A. E. *Austral. J. Earth Sci.* **35,** 59-72 (1988).
53. Christie-Blick, N., Grotzinger, J. P. & von der Borch, C. C. *Geology* **16,** 100-104 (1988).
54. Christie-Blick, N., von der Borch, C. C. & DiBona, P. A. *Am. J. Sci.* **290A,** 295-332 (1990).
55. Ross, G. M. & Murphy, D. C. *Geology* **16,** 139-143 (1988).
56. Preiss, W. V., Walter, M. R., Coats, R. P. & Wells, A. T. *BMR J. Aust. Geol. Geophys.* **3,** 43-53 (1978).
57. Cowie, J. W. & Harland, W. B. in *The Precambrian-Cambrian Boundary* (eds Cowie, J. R. & Brasier, M. D.) 186-204 (Clarendon, Oxford, 1989).
58. Compston, W. *et al. Res. Sch. Earth Sci. Aust. Nat. Univ. A. Rep.* **1990,** 26-27 (1990).
59. Jenkins, R. J. F. *Geol. Mag.* **121,** 635-643 (1984).
60. Conway Morris, S. in *The Precambrian-Cambrian Boundary* (eds Cowie, J. R. & Brasier, M. D.) 7-39 (Clarendon, Oxford, 1989).
61. Plumb, K. *Episodes* **14,** 139-140 (1991).
62. Sokolov, B. S. *Izv. Akad. nauk SSSR ser. geol.* **5,** 21-31 (1952)
63. Jenkins, R. J. F. *Trans. R. Soc. S. Aust.* **105,** 179-194 (1984).
64. Harland, W. B. & Herod, K. M. in *Ice Ages: Ancient and Modern* (eds. Wright, A. E. & Moseley, F.) 189-216 (Steel Horse, Liverpool, 1975).
65. Whittaker, A. *et al. J. geol. Soc. Lond.* **148,** 813-824 (1991).

ACKNOWLEDGEMENTS. We thank L. Smith, S. Grant, S. Conway Morris, P. Link, W. B. Harland, J. Veevers and R. Jenkins for comments. This work was supported by NASA, NSF and a Visiting Fellowship from Gonville and Caius College, Cambridge (A.H.K.); and the Australian Research Council (M.R.W.)

Upper-mantle seismic discontinuities and the thermal structure of subduction zones

John E. Vidale & Harley M. Benz

United States Geological Survey, Branch of Seismology, 345 Middlefield Road, MS 977, Menlo Park, California 94025, USA

The precise depths at which seismic velocities change abruptly in the upper mantle are revealed by the analysis of data from hundreds of seismometers across the western United States. The boundary near 410 km depth is locally elevated, that near 660 km depressed. The depths of these boundaries, which mark phase transitions, provide an *in situ* thermometer in subduction zones: the observed temperature contrasts require at least moderate thickening of the subducting slab near 660 km depth. In addition, a reflector near 210 km depth may mark the bottom of the aesthenosphere.

OUR understanding of the composition, convective pattern and temperature field in the Earth's mantle is derived from many kinds of geophysical evidence. The radial seismic structure is an important clue to the dynamics of the mantle. At least two depths in the mantle are known from seismology to be the location of transitions in rock properties. Near 410 km depth, the transition from the α to the β phase of olivine (hereafter referred to as the '410') is identified by a 5% increase in shear and compressional velocity and density. Near 660 km depth (hereafter the '660'), the P and S velocities and density again increase by ~5%, consistent with the transition from γ-phase olivine to perovskite plus magnesiowüstite[1,2], and perhaps an increase in iron and silica content.

There is continued debate as to whether the mantle convects in a single system from crust to core, or whether mantle convection is stratified, with the '660' inhibiting mass transport between the upper and lower mantle[2,3]. Many details remain unresolved. Measurement of the sharpness, contrast and depth variations of both the '410' and '660' boundaries can contribute to estimating the lateral temperature contrasts as well as the composition of the mantle.

Measurements of the '410' and '660' boundaries have been made with a variety of seismic techniques. These boundaries generate reflections and conversions, as well as more complicated arrivals near the critical angle. Generally, long-period studies measure boundary depths and impedance contrasts more precisely, whereas short-period studies have greater resolution of short-wavelength features such as sharpness and lateral depth variation. The '410' and '660' were discovered from studies of seismic body waves recorded at distances between 10 and 35° from earthquakes. Within part of this range, for each boundary, it is possible to observe an arrival that travelled above the discontinuity, an arrival that was reflected by the discontinuity and an arrival that penetrated below the discontinuity[4].

Global observations of the '410' and '660' discontinuities have been obtained from reflected waves of 25-50 s period[2,5,6]. The lateral resolution of these waves is ~1,000 km. The temperature field near subducting slabs, however, is expected to show shorter-wavelength variations, because of the ~100-km scale length of thermal diffusion of lithosphere subducted 10 million years ago. Temperature variations are expected to result in variations in the depth of both the '410' and '660' boundaries. Consequently,

shorter-period seismic waves are necessary to measure these shorter-wavelength boundary deflections.

In contrast to previous work, here we use a large-aperture array with many elements, each of which is a short-period seismometer. Array study of the waveforms improves the signal-to-noise ratio by the cancellation of the near-receiver reverberations and other noise, which differ for each station. We examine one earthquake at a time to find mantle reflections that leave the source region in a fairly narrow cone of take-off angles. Our measurements sample mantle structures across a lateral extent of only a few tens of kilometres, giving much higher resolution than previous work.

The large-aperture dense array

The five regional, short-period arrays whose seismograms we examine are the Northern California Seismic Network, the Southern California Seismic Network, the University of Utah Regional Seismic Network, the University of Nevada-Reno Seismic Network and the Washington Regional Seismic Network. Combined, the arrays consist of 881 short-period vertical stations across the western United States (Fig. 1). The resulting antenna, which spans 1,700 km by 800 km, covers more than 30 times the area of the short-period arrays previously used for mantle waveform studies. From six earthquakes, we observe mantle reflectors beneath South America, Tonga, Bonin and Mariana with roughly the geometry shown in Fig. 2. These earthquakes are recorded with good signal-to-noise ratios at frequencies between 0.2 and 5.0 Hz.

With the spacious aperture and the multiplicity of stations, we can effectively eliminate the largest sources of noise, which are microtremor, electronic noise and near-station reverberations. The scattering near the source is minimized by considering the part of the wavefield that arrives before pP, the earliest arriving energy scattered off the Earth's surface or ocean bottom above the source.

The seismograms that we analyse contain most of their energy at a period of 4 s. Although the instruments are designed to measure shorter-period seismic energy, they have been used to study ground motion up to 20–30 s period[7]. We visually examine every trace and reject the 40–70% that are too noisy or dissimilar to nearby stations. A time in the P or pP arrival is handpicked, either the onset time or a prominent early peak, depending on

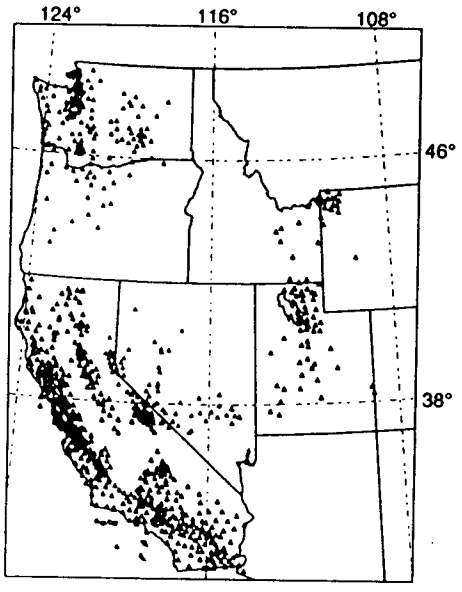

FIG. 1 Location of the 881 stations in the five regional short-period arrays assembled in this study.

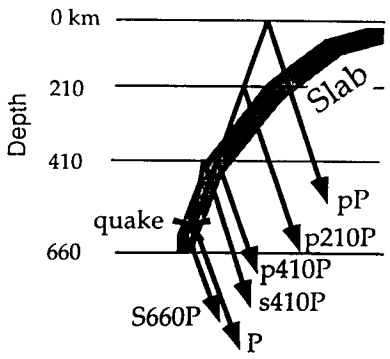

FIG. 2 Typical geometry of an earthquake and the structures that we observe. The shaded region marks the trend of the earthquakes that define the Wadati–Benioff zone.

the character of the earthquake. The traces are shifted in time so that the picked phase arrives at the same time for all traces, normalized to a peak amplitude of unity and searched for plane wave arrivals.

We do not combine earthquakes because the mechanisms and rupture time histories vary, and also we do not assume that each earthquake will illuminate the same structures. We do not cross-correlate to isolate secondary arrivals, as some of the arrivals we seek initially travel upwards, others downwards; some energy emerges from the source region as an S wave, some as a P wave. Only for cases in which the source is small compared to the seismic wavelengths is cross-correlation or deconvolution effective[2,6].

The earthquake depth is required to estimate the depth of the reflectors imaged here. The uncertainty in earthquake depth is least for the four events relocated with both pP and P arrivals as part of an inversion for three-dimensional slab structures[8]. The difference in earthquake depth between locations in a one-dimensional and a three-dimensional velocity model is ~1 km (ref. 8). The uncertainty in earthquake depth is difficult to state precisely, but is probably less than 10 km.

The depth uncertainty is greater for the two events taken from the International Seismic Centre (ISC) catalogue. These depths are probably accurate to ±15 km, depending mostly on whether the correct pP phases were chosen and on the accuracy of the assumed velocity structure above the earthquake[9]. For example, ISC depth estimates using the pP − P times are 5 km deeper on average than depths determined using P times alone, and differences between the two depths have a variance of 11 km. The errors in the two measurements are largely independent, as errors in P locations mostly depend on velocity anomalies beneath the earthquakes whereas errors in pP − P locations mainly depend on velocity anomalies above the earthquakes.

Figure 3*a* and *b* compares data and synthetic seismograms for 70 of the 279 waveforms analysed from the 3 April 1985 event, which is near 476 km depth in the Bonin subduction zone. It is clear that the signals we seek are small compared with the P-wave coda and that we must stack many records to resolve the weak reflections expected from the upper-mantle discontinuities.

A slant stack, also called a radon transform by mathematicians and a p–τ stack in the oil industry, resolves plane-wave arrivals while minimizing incoherent signals. A point in the slant stack represents the sum along a line through a seismic section such as those shown in Fig. 3*a* and *b*. Each line is described by its slowness (reciprocal of apparent velocity) across the array and its delay time when the line intersects a reference station. Figure 3*c* and *d* compares the stacks at the P-wave slowness for the data and the synthetic seismograms. Figure 3*e* and *f* compares the stacks at the pP slowness. The stacking process has reduced the noise enough that we can see a minor arrival 20 s after the

TABLE 1 Earthquakes

Date	Region	Depth (km)	Latitude (N)	Longitude (E)	Mag	'660' depth	'410' depth	'210' depth
28 April 1981	Tonga	540*	−23.7°	180.0°	6.0	685	387	208
4 Janary 1982	Mariana	606*	18.0°	145.6°	6.1	—	408	214
3 April 1985	Bonin	476*	28.2°	139.5°	6.0	677	—	207
16 June 1986	Tonga	559*	−22.0°	−178.9°	6.3	690	398	202
27 October 1987	South America	604†	−28.7°	−62.9°	6.0	686‡	406	220
3 May 1991	Bonin	462†	28.0°	139.6°	6.0	686	—	215

* Depth from relocation and velocity inversion[8].
† Depth from pP−P location (PDE Bulletin).
‡ Depth from 2-s rather than 4-s period slant stack.

P wave, but only in the stack at the P-wave slowness. This arrival, as well as the energy 60 s after P, will be interpreted below. The pP arrival is noticeably more complicated than the P arrival in the data, probably because of the water layer and structural complexity where pP reflects from the surface of the Earth.

Figure 4 shows the logarithm of the envelope of the slant stacks of records from this earthquake. The envelope is the amplitude of the analytical slant-stack time series and serves only to eliminate the four or five zero crossings in each arrival apparent in Fig. 3*c* and *e*. The use of the logarithm with colour allows a factor of 100 variation in amplitude to be presented.

Many arrivals can be seen in Fig. 4. Note that the window between P and pP is very clean, so that signals with amplitudes from 2 to 10% of the direct P wave can be identified. The arrivals are unlikely to be aftershocks because most arrive with slownesses different from the main shock. The similarity of the sequences of arrivals following earthquakes in similar locations also argues against their interpretation as aftershocks.

The signal-to-noise levels are similar for slant-stacks of period 1, 2 and 4 s. It seems that the improved instrument response at shorter periods is offset by larger-amplitude scattered waves and less coherence across the array. The stacks for 4-s period show most clearly the signals from the '410' and '660' reflectors, as well as a signal reflecting near 210 km depth.

Identification of mantle reflections

Four earthquakes show the arrival that travels out from the source as an S wave and converts to a P wave near 660 km depth. A fifth event, indicated in Table 1, only shows a clear arrival at higher frequency. Figure 5 shows the slant stacks of the P wave and the following 30 s for the four events. The traces are aligned so that an S-to-P conversion at 660 km depth would appear centred on the purple vertical line. An arrival appears for each event ~2–3 s later than expected. The amplitude of this arrival is ~10% of the direct P wave, in accord with the prediction of synthetic seismograms.

Arrival times of these S-to-P conversions correspond to reflector depths of 677, 685, 686, 686 and 690 km (Table 1). These depths were calculated by solving for the location of a flat reflector that produces an S-to-P converted arrival with the observed delay time after the direct P wave. Other possible origins include P-to-P reflections from a horizon that varies between 340 and 500 km depth, S-to-P reflections from a horizon that varies between 380 and 520 km depth, or reflections from dipping surfaces. The consistency of depths, the prediction of such arrivals in reflectivity synthetics and the observation that these arrivals generally show slightly steeper angles of incidence than the direct P wave, as expected for S-to-P conversions in transmission, rather than the slightly less steep angles of incidence expected for reflections and conversions above the source, indicate that the first explanation is correct. The uncertainty in these boundary depth estimates would be less than 10 km, mainly due to the possibility of some dip in the boundary, if the exact depth of the earthquake were precisely known.

The events in Tonga produce '660' depths of 685 and 690. Earlier work on earthquakes with similar focal depths suggested that this boundary was roughly 10 km shallower[11]. Our earthquake depths, based on pP−P measurements and three-dimensional upper- and lower-mantle velocity structure[8], are more accurate. The previous work[11] measures arrivals that contain energy at <1 s period, whereas we use arrivals of 4 s period. Their arrivals convert nearer the deep seismicity than the arrivals that we examine, as the array that they examine is in Australia whereas ours is in North America. Their array aperture is ~10 km; ours is 1,500 km, allowing greater slowness resolution, although their study has many more events at various depths. We stack seismograms for one event at a time; they stack envelopes for multiple events, so our study is more sensitive to structure that varies laterally. Given these differences, it is not surprising that slightly different depths for the '660' are found.

The slant stacks for all six events are shown in Fig. 6. The primary arrivals, P and pP, appear red and yellow; they have high amplitude and are well defined. The purple triangles above the upper four stacks locate the S'660'P arrivals that were shown in more detail in Fig. 5. For four events, an arrival that we identify as p'410'P is marked by the blue triangles. It may also be present for the other two events, but would be obscured by S'660'P. This reflector, measured with the assumption of horizontal layering, lies at depths of 387, 398, 406 and 408 km for the four events. If these reflections were S-to-P conversions

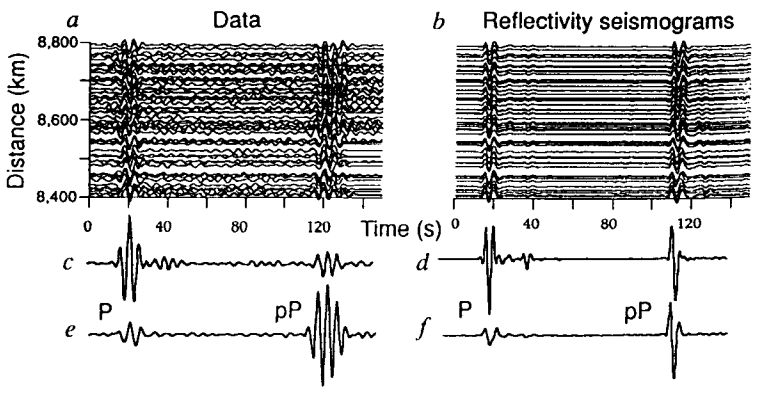

FIG. 3 *a*, Seismograms from 70 of the 279 stations used to study the 3 April 1985 earthquake, which cover only a quarter of the aperture of our array. All seismograms are aligned on the pP phase. *b*, Reflectivity seismograms for the same 70 stations. The IASP91 velocity model is used[31], and the centroid moment tensor mechanism[32] is assumed. The synthetics are filtered in the same way as the data. *c*, *d*, Stacks of the data and reflectivity seismograms with the P arrivals aligned. *e*, *f*, Stacks of the data and reflectivity seismograms with the pP arrivals aligned.

which have 30 km wavelength, requires that the reflector be less than a quarter wavelength (8 km) thick.

Cause of reflectors at 210, 400 and 680 km

The five observations of upper-mantle seismic discontinuities near 660 km depth suggest that the γ-phase olivine to perovskite plus magnesiowüstite boundary is depressed by 20–30 km compared to global averages based on long-wavelength measurements[2,5,6]. This variation is somewhat greater than the 20-km depression observed to the northwest of subduction in the northwest Pacific with long-period shear waves[2], whose resolution is ~1,000 km. The resolution of our high-frequency observations is an order of magnitude finer because we are using waves five times higher in frequency and because the conversion point is near the source rather than near the midpoint of the ray path. We sample the '660' about 100 km from the intersection of the seismicity that defines the Wadati–Benioff zone and 660 km depth, toward the direction from which the subducting lithosphere is approaching (the right, in Fig. 2). The '660' boundary in this direction has been estimated to lie at a more normal depth than on the other side in the Kurils[2]. We therefore observe more depth variation than is seen with longer-wavelength probes. Depression of the boundary by 25 km suggests a decrease in temperature of ~300 °C (±30%)[11]. And this elevation is measured outside the region where simple models of throughgoing subducting slabs place the core of the slab[12], requiring that the thermal anomaly be spread by broadening of the slab rather than by thermal conduction alone.

The four observations of upper-mantle seismic discontinuities near 410 km depth suggest that the α-to-β phase boundary is elevated by ~15 km near the core of subducting slabs. Our reflection points range from the middle of the seismicity at 410 km depth to ~100 km to the side of the seismicity. As our observations are made in areas above deep earthquakes, we are measuring the depth of the phase transition either in material that is subducting or that has been next to subduction for a long time. An elevation of the equilibrium $\alpha \rightleftharpoons \beta$ phase boundary of 15 km would result from 400 °C (±30%) difference in temperature between subduction zones and normal mantle[13,14]. This is less than the expected thermal anomaly in the core of the slab. But as the wavelength of features that can be resolved in this study is 50–100 km, we still may not be observing the full elevation of the discontinuity if the coldest zone is narrow.

Mineral physics experiments show that the $\alpha \rightleftharpoons \beta$ phase transition is kinetically hindered at temperatures below 520–900 °C, at least on laboratory timescales[15]. Seismic studies have suggested that the depth of this transition is depressed near slabs[16], is elevated[17,18] or has no measurable deflection[5], and a small anticorrelation between the depth to the 660 and 410 km discontinuities has been observed[6]. Our observations of a boundary elevated by 15 km suggest that the phase transition can proceed at temperatures 400 °C colder than ambient mantle[13]. It is still possible that isolated pockets of olivine remain untransformed, or that the cold centre of the slab forms a thin, untransformed tongue of metastable olivine.

Recent work indicates that this transition may initiate and lubricate deep earthquakes, overcoming the high friction theoretically expected to prevent seismic faulting[19,20]. Our results indicate that the transformation progresses at temperatures several hundred degrees colder than the normal mantle geotherm. If metastability is to account for deep earthquakes, it must persist to near 660 km depth, despite the adiabatic temperature increase of ~200 °C from 410 to 660 km depth[13]. Alternatively, some compositional or grain-size influence on metastability may allow the penetration of the α phase to the depths of the deepest earthquakes, but this seems unlikely.

Published observations and interpretations of a seismic velocity discontinuity near 210 km depth span the past 30 years[5,7,21,22]. Long-period, wide-angle seismic profiles have often been interpreted to show structures near 210 km depth. A velocity increase near 200 km depth underlain by a minor velocity decrease is seen beneath Australia[23], but the sharpness is difficult to resolve. A velocity decrease near 160 km depth, underlain by an increase in velocity near 190 km, is inferred beneath northwestern Eurasia[24]. These two studies examined areas beneath stable continents. A large velocity contrast underlies Japan, somewhat shallower than 200 km depth[25]. Under Tibet, a reflector is observed near 200 km depth[26].

Reflections from near 210 km depth are not seen by recent long-period shear-wave studies[5,27] under oceans; the present study, however, has the advantage of a more favourable signal-to-noise ratio, more localized sampling and more sensitivity to moderately dipping reflectors. Another explanation of this discrepancy would be that the reflector is laminated, with little long-period signature. Perhaps the feature is confined to a small area around subduction zones. But the volume of literature reporting seismic velocity changes near 210 km depth suggests that a global boundary may be present.

The nature of the reflector required by Fig. 6 is not simple to deduce. A depth of 210 km has been proposed as the level of a compositional boundary[22,28]. The constancy of depth adjacent to subduction zones, where material passes through the 210-km level, is difficult to reconcile with a compositional boundary. This depth has also been proposed as the bottom of partial melting, which would correspond to the base of the low-velocity zone, and this is the most likely interpretation. A discontinuity near this depth has been proposed as the base of the lid beneath continents, but it seems to lie deeper and mainly beneath older continents[27], whereas we observe the structure beneath oceans.

The reflections from the '410' show that the $\alpha \rightarrow \beta$ boundary is elevated by ~15 km within cold, subducting material, consistent with a temperature anomaly of ~400 °C. This amount of relief on the boundary argues against penetration of metastable olivine to the depth of the deepest earthquakes. The 25-km depression of the boundary at which the γ-phase of olivine transforms to perovskite plus magnesiowüstite is greater than that observed at longer wavelength, and consistent with temperatures 300 °C colder than normal. Such temperature contrasts are about twice as large as those inferred from large-scale global variations of discontinuity depth. Measurements of long-period shear waves[5,6] find ~15 km of depth variation (zero to peak) for the '660' and 5–10 km for the '410'. These studies indicate lateral variations of ~100 °C. Lateral compressional-wave velocity variations have been interpreted to indicate 120 (±100) °C temperature variations in the mid-mantle[28].

Temperature variations of 300–400 °C are consistent with thermal models of slabs. The core of the slab may be ~800 °C colder than ambient mantle[12], so a contrast of 400 °C at 410 km depth is the result one would expect from this fairly long-wavelength probe. Near the '660', it is more difficult to know what temperature contrast to expect ~100 km towards the direction of approach of the subducting plate. The simplest, narrowest slab models[12,20] predict only a small temperature perturbation at our S'660'P conversion point. The models in which viscosity increases by more than a factor of 10 below the '660' (ref. 30) and the models in which the anomalously cold zone is broad[12] do predict a few hundred degrees of anomaly, as we observe. □

Received 30 December 1991; accepted 24 March 1992.

1. Jeanloz, R. *Geophys. Res. Lett.* **18**, 1743–1746 (1991).
2. Shearer, P. M. & Masters, T. G. *Nature* **355**, 791–795 (1992).
3. Silver, P. G., Carlson, R. W. & Olson, P. *A. Rev. Earth planet. Sci.* **16**, 477–541 (1990).
4. Helmberger, D. V. & Engen, G. *J. geophys. Res.* **79**, 4017–4029 (1974).
5. Shearer, P. M. *J. geophys. Res.* **96**, 18147–18182 (1991).
6. Revenaugh, J. & Jordan, T. H. *J. geophys. Res.* **96**, 19763–19780 (1991).
7. Wald, L. A. & Heaton, T. H. *J. geophys. Res.* **96**, 12099–12125 (1991).
8. Van der Hilst, R., Engdahl, E. R., Spakman, V. & Nolet, G. *Nature* **353**, 37–43 (1991).
9. Stark, P. B. & Frohlich, C. *J. geophys. Res.* **90**, 1859–1869 (1985).
10. Richards, M. A. & Wicks, C. W. Jr *Geophys. J.* **101**, 1–35 (1990).
11. Ito, E. & Takahashi, E. *J. geophys. Res.* **94**, 10637 (1989).
12. Fischer, K., Creager, K. & Jordan, T. H. *J. geophys. Res.* **93**, 4773 (1988).
13. Akaogi, M., Ito, E. & Navrotsky, A. *J. geophys. Res.* **94**, 15671–15688 (1989).
14. Katsura, T. & Ito, E. *J. geophys. Res.* **94**, 15663–15671 (1989).

15. Sung, C. M. & Burns, R. G. *Earth planet. Sci. Lett.* **32**, 165-170 (1976).
16. Iidaka, T. & Suetgetsu, D. *Nature* (in the press).
17. Solomon, S. C. & U, K.T.P. *Phys. Earth planet. Sci. Lett.* **11**, 97-108 (1975).
18. Helffrich, G. R., Stein, S. & Wood, B. J. *J. geophys. Res.* **94**, 753-763 (1989).
19. Green, H. W. & Burnley, P. C. *Nature* **341**, 733-737 (1989).
20. Kirby, S. H., Durham, W. B. & Stern, L. A. *Science* **252**, 216-225 (1991).
21. Lehmann, I. *Ann. Geophys.* **15**, 93-118 (1959).
22. Anderson, D. L. *J. geophys. Res.* **84**, 7555-7561 (1979).
23. Bowman, J. R. & Kennett, B. L. N. *Geophys. J. Int.* **101**, 355-366 (1990).
24. Given, J. W. & Helmberger, D. V. *J. geophys. Res.* **85**, 7183-7184 (1980).
25. Kanamori, H. *Bull. Earthquake Res. Inst.* **45**, 657 (1967).
26. Kato, M. & Hirahara, K. *Geophys. J. Int.* **106**, 551-558 (1991).
27. Revenaugh, J. & Jordan, T. H. *J. geophys. Res.* **96**, 19781-19810 (1991).
28. Anderson, D. L. & Bass, J. *Nature* **320**, 321-328 (1986).
29. Gurnis, M. & Hager, B. H. *Nature* **335**, 317-321 (1988).
30. Duffy, T. & Ahrens, T. J. *J. geophys. Res.* (in the press).
31. Kennett, B. L. N. *IASPI 1991 Seismological Tables* (Research School of Earth Sciences, Australia National Univ., 1991).
32. Dziewonski, A. M. & Woodhouse, J. H. *J. geophys. Res.* **88**, 3247-3271 (1983).

ACKNOWLEDGEMENTS. We thank Q. Williams, T. Lay, H. Houston, E. Knittle and W. Ellsworth for discussions, P. Shearer and E. R. Engdahl for helpful reviews, the Lamont-Doherty Geological Observatory, J. Evans, B. Julian, A. Walter and J. Luetgert for software, R. Somera, J. Mori, R. Benson, S. Nava and D. Depaulo for assistance in recovering data, and E. R. Engdahl and R. Van der Hilst for providing unpublished depths for four earthquakes.

Successive action of DnaK, DnaJ and GroEL along the pathway of chaperone-mediated protein folding

Thomas Langer*, Chi Lu†, Harrison Echols†, John Flanagan‡, Manajit K. Hayer* & F. Ulrich Hartl*§

* Program in Cellular Biochemistry and Biophysics, Rockefeller Research Laboratories, Sloan-Kettering Institute, 1275 York Avenue, Box 520, New York, New York 10021, USA
† Department of Molecular and Cell Biology, University of California, Berkeley, California 94720, USA
‡ Department of Molecular Biophysics and Biochemistry, Yale University, New Haven, Connecticut 06511, USA

The main stress proteins of *Escherichia coli* function in an ordered protein-folding reaction. DnaK (heat-shock protein 70) recognizes the folding polypeptide as an extended chain and cooperates with DnaJ in stabilizing an intermediate conformational state lacking ordered tertiary structure. Dependent on GrpE and ATP hydrolysis, the protein is then transferred to GroEL (heat-shock protein 60) which acts catalytically in the production of the native state. This sequential mechanism of chaperone action may represent an important pathway for the folding of newly synthesized polypeptides.

PROTEINS can fold *in vitro* without the help of additional components, demonstrating that the amino-acid sequence contains the full information to specify the native conformation[1,2]. It was therefore assumed that the folding of proteins *in vivo* occurred by an essentially spontaneous process as well. But then it was discovered that the folding of certain newly synthesized proteins depends on so-called 'molecular chaperones'[3], or 'polypeptide chain binding proteins'[4]. These proteins have the ability to interact with many unfolded or partially denatured proteins apparently without specific recognition of defined sequence motifs. The involvement of molecular chaperones in *de novo* protein folding has been established for the constitutively expressed stress proteins of the heat-shock proteins Hsp70 and Hsp60 families[5-8]. Defining the functions of these components will be crucial for understanding the mechanisms of protein folding within cells.

Although structurally unrelated, members of both classes of molecular chaperones use the energy of ATP hydrolysis to release bound substrate proteins. The Hsp70s probably act as monomers or dimers, whereas the Hsp60s (the so-called chaperonins[9]) are functional as high-molecular-weight oligomeric structures that are composed of two stacked seven-subunit rings. Members of the Hsp70 family are involved in diverse functions, including maintaining proteins in an unfolded state[10-13], dissociating protein aggregates, and facilitating renaturation[5,14,15]. The Hsp70 homologue of *E. coli*, DnaK, cooperates functionally with two additional heat-shock proteins, DnaJ and GrpE (refs 16-18). Members of the Hsp60 family *in vivo* and *in vitro* mediate the folding of proteins to the native structure and facilitate oligomeric protein assembly[19-29]. Folding may occur by a process of stepwise ATP-dependent release from the oligomeric GroEL structure[28].

Studies on the cellular functions of heat-shock proteins have focused mainly on one class of components, so we do not yet have an integrated view of the roles of the different chaperone families in protein folding. Hsp70s and Hsp60s seem to interact with different structural elements of unfolded polypeptides. Consistent with their binding to nascent chains[30], members of the Hsp70 family interact with synthetic peptides[31] and with polypeptides in extended conformations[32]. In contrast, the Hsp60 of *E. coli*, GroEL, may recognize secondary structure elements[33] and stabilize bound proteins as conformational intermediates formed early in folding, like the 'molten globule'[28]. That division of labour between Hsp70s and Hsp60s is physiologically significant is shown by the folding of proteins in mitochondria. During import from the cytosol, precursor proteins traverse the mitochondrial membranes as extended chains[34]. The newly translocated polypeptides first interact with the DnaK-related Hsp70 in the mitochondrial matrix[35-37]. For a number of proteins this interaction is necessary but not sufficient for folding and assembly, which depend on the subsequent transfer of the polypeptide chains to Hsp60 (refs 19, 21, 37), the mitochondrial GroEL homologue[38]. A DnaJ-like activity may participate in the process, given that a DnaJ-related protein has recently been identified that is possibly localized in mitochondria[39].

As the chaperone proteins of mitochondria have homologous equivalents in the *E. coli* cytosol, it may be that the pathways of chaperone-mediated protein folding in both compartments

§ To whom correspondence should be addressed.